IEEE Open Journal of
Power Electronics

Received 1 December 2025; revised 7 January 2026; accepted 14 January 2026. Date of publication 27 January 2026;
date of current version 9 February 2026. The review of this article was arranged by Associate Editor Hongbo Zhao.

Digital Object Identifier 10.1109/OJPEL.2026.3658028

Robust Control Strategies for Grid-Connected Crossover Switches Cell Multilevel Inverters: Comparative Analysis and Performance Evaluation

HAMZA MAKHAMREH [1] (Senior Member, IEEE), MOHAMED TRABLESI [2] (Senior Member, IEEE), AND HANI VAHEDI [3,4] (Senior Member, IEEE)

[1]Özyeğin University, Istanbul 34794, Türkiye
[2]Kuwait College of Science and Technology, 72304, Kuwait
[3]Abdullah Al Salem University, 92204, Kuwait
[4]Delft University of Technology, 2628 Delft, The Netherlands

CORRESPONDING AUTHOR: HAMZA MAKHAMREH (e-mail: hamza.makhamreh@ozyegin.edu.tr)

The work was supported by the Kuwait Foundation for the Advancement of Sciences (KFAS) under Project CN23-13EE-1882.

ABSTRACT Multilevel inverters (MLIs) have become key enablers in renewable energy (RE) integration and electric vehicle (EV) systems, where high-quality power conversion and robustness are critical. Among the different topologies, the Crossover Switches Cell (CSC) converter has recently gained attention due to its superior voltage-boosting capability and reduced component count. While most existing studies on CSC control strategies have been limited to simulations, this work advances the field by providing comprehensive real-time experimental validation under varying operating conditions and parameter mismatches. Finite Control Set Model Predictive Control (FCS-MPC), Sliding Mode Control (SMC), and Lyapunov-based MPC (LMPC) are comparatively assessed in terms of dynamic response, voltage regulation, harmonic minimization, and robustness. Real-time implementation on an Opal-RT platform demonstrates that MPC achieves superior current control with minimal harmonics, SMC offers strong disturbance rejection and effective capacitor voltage balancing, while LMPC guaranties stability with a reduced computational burden. The presented results highlight the trade-offs between these advanced control strategies while providing practical guidelines for selecting robust control techniques for grid-connected MLIs in RE and EV applications.

INDEX TERMS Sliding mode control, model predictive control, lyapunov stability, crossover switches cell, multilevel inverters, radar area indicator.

I. INTRODUCTION

Nowadays, power electronics technology serves as a key enabler for advancing renewable energy (RE) integration, electric vehicle (EV) technologies, and energy storage systems (ESSs) [1], [2].

Multilevel inverters (MLIs) are the cornerstone of advanced power electronics, characterized by generating high-quality multilevel voltage waveforms [3], [4], [5] with reduced total harmonic distortion (THD) and electromagnetic interference (EMI). Recent studies have highlighted the advancements in these technologies, pushing the boundaries of power electronics performance and application. Among the most recognized MLI topologies are Neutral Point Clamped (NPC) inverters, which utilize diodes to clamp the neutral point and achieve voltage levels, thus minimizing voltage stress and harmonic distortion [6]. The Modular Multilevel Converter (MMC) stands out for its scalability and high efficiency, especially suited for high-voltage applications such as HVDC power transmission and variable speed drives [7], [8]. Flying Capacitor Inverters (FCIs), another prominent topology, leverage multiple capacitors to achieve different voltage levels, allowing for flexible voltage management and redundancy in power conversion [9], [10]. Recently, Packed U-cell (PUC) inverters [11], [12], characterized by their

compact design and reduced component count, have emerged as an asymmetrical version of FCIs, offering an efficient solution for medium-voltage applications. Furthermore, the CSC converter, a modified version of PUC inverters, enhances this efficiency by introducing additional switching elements that allow for greater control and flexibility in voltage levels [13].

The CSC has been subjected to various control techniques to optimize its performance in applications ranging from RE integration to EV applications. On the one hand, Sliding Mode Control (SMC), renowned for its robustness against system uncertainties and external disturbances, has been a popular choice for controlling CSC converters. This method employs a discontinuous control action to drive the system states to a predefined sliding surface and maintain it thereafter, ensuring system stability and reduced sensitivity to parameter variations. Recent applications of SMC on CSC converters have demonstrated improved dynamic responses and reduced chattering, a common issue with traditional SMC implementations. The work published in [14] showcases significant enhancement in reducing total harmonic distortion (THD) and improving the overall efficiency of the system. In the context of modular multilevel converters, the sliding mode control and virtual impedance loop are introduced to strengthen system robustness in [15].

On the other hand, Model Predictive Control stands out for its ability to handle multivariable control problems and predict future system states, making it extremely effective for managing the complex dynamics of CSC converters. By formulating a cost function that evaluates future states based on a set of possible control actions, MPC can optimize the switching states to minimize power losses and improve voltage quality. The authors in [16], [17] explored the application of MPC on CSC converters, highlighting its high performance in achieving fast response and low THD.

Besides, Lyapunov-based control strategies involve designing a control law from the Lyapunov stability perspective. In the context of CSC converters, this approach ensures that the voltage and current levels remain within safe operating limits. The study presented in [18] on Lyapunov-based MPC for a 9-level CSC converter points out its effectiveness in enhancing the robustness and maintaining stability while eliminating the need for gain tuning, thereby simplifying the implementation process.

Thus, this paper investigates the application of MPC, SMC, and LMPC to a grid-connected 9-level CSC converter, addressing both their implementation challenges and performance trade-offs. Unlike prior studies that focused primarily on simulation, this work provides a comprehensive assessment through real-time experimental validation on an Opal-RT platform under steady-state, transient, and parameter mismatch conditions. The controllers are benchmarked in terms of dynamic response, harmonic performance, and robustness against uncertainties. By combining detailed simulation with experimental insights, this comparative study offers practical guidelines for selecting suitable control strategies for grid-connected MLIs, thereby advancing the optimization of robust control solutions in power electronics.

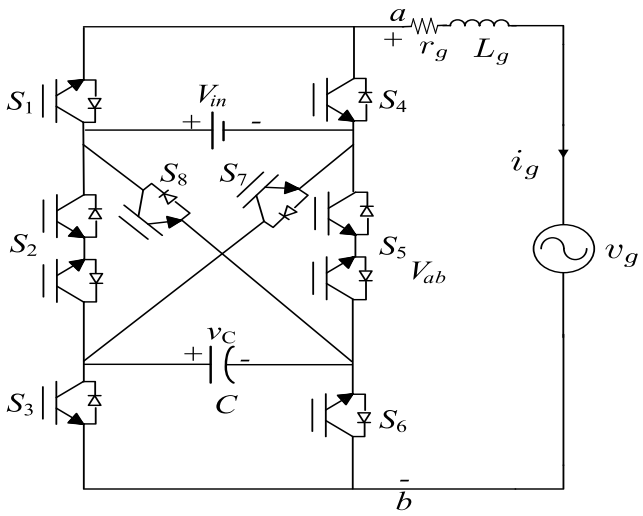

FIGURE 1. Grid-tied Crossover Switches Cell Multilevel Inverter.

II. MATHEMATICAL MODELLING AND OPERATION OF CROSSOVER SWITCHES INVERTER

The 3-cell Crossover Switches Cell Converter, illustrated in Fig. 1, is a modified version of the 3-cell Packed U-Cell converter. This modification involves the addition of two extra switches, strategically placed across the input DC voltage on one side and the flying capacitor on the other. These added switches enhance the voltage boosting capability by creating additional pathways for the charging and discharging processes. Another key advantage of the CSC converter over the traditional PUC inverter is its ability to generate more voltage levels. Specifically, when the flying capacitor voltage is set to one-third of the DC input voltage, the 3-cell CSC converter achieves up to nine distinct voltage levels, whereas the PUC inverter version is limited to seven levels.

The converter depicted in Fig. 1 can be reconfigured into two parallel branches: one consisting of a half-bridge inverter and the other incorporating a flying capacitor, both connected in parallel with the DC source. In this configuration, the upper switch (S_2) and lower switch (S_5) enable bidirectional current flow, enhancing the system's flexibility. Additionally, two cross switches (S_8 and S_7) establish connections between the positive and negative terminals of the DC supply and the corresponding opposite terminals of the flying capacitor. The switching operation follows a complementary pattern, where S_1, S_2, and S_3 operate inversely with S_4, S_5, and S_6, respectively. To maintain proper switching sequences and avoid conflicts, only one switch from the set (S_2, S_5, S_7, S_8) can be in the ON state at any given time, as specified in Table 1.

If the input DC voltage (V_{in})is assumed to be $3E$, and the FC reference voltage is E, then the output voltage varies from 0, $\pm E$, $\pm 2E$, $\pm 3E$, and $\pm 4E$ for different switching states

TABLE 1 Possible Switching States for CSC Converter

i	S_1	S_2	S_3	S_4	S_5	S_6	S_7	S_8	s_a	s_b	v_{ab}	v_C
1	1	0	0	0	0	1	1	0	1	1	$v_{in}+v_C$	↑↑
2	1	0	0	0	1	1	0	0	1	0	v_{in}	∼∼
3	1	0	1	0	0	0	1	0	1	0	v_{in}	∼∼
4	1	0	1	0	1	0	0	0	1	-1	$v_{in}-v_C$	↓↓
5	0	0	0	1	0	1	1	0	0	1	v_C	↑↑
6	1	1	0	0	0	1	0	0	0	1	v_C	↑↑
7	0	0	1	1	0	0	1	0	0	0	0	∼∼
8	1	1	1	0	0	0	0	0	0	0	0	∼∼
9	0	0	0	1	1	1	0	0	0	0	0	∼∼
10	1	0	0	0	0	1	0	1	0	0	0	∼∼
11	0	0	1	1	1	0	0	0	0	-1	$-v_C$	↓↓
12	1	0	1	0	0	0	0	1	0	-1	$-v_C$	↓↓
13	0	1	0	1	0	1	0	0	-1	1	$-v_{in}+v_C$	↑↑
14	0	0	0	1	0	1	0	1	-1	0	$-v_{in}$	∼∼
15	0	1	1	1	0	0	0	0	-1	0	$-v_{in}$	∼∼
16	0	0	1	1	0	0	0	1	-1	-1	$-v_{in}-v_C$	↓↓

↑: charging, ↓: discharging, ∼: bypassing.

$i = 1, \ldots 16$. The switch S_x is turned ON and OFF as

$$s_i = \begin{cases} 1, & \text{if } S_x \text{ is ON} \\ 0, & \text{if } S_x \text{ is OFF.} \end{cases} \tag{1}$$

The controller design and operation of the grid-connected CSC inverter can be simplified if one defines the following mathematical function as

$$\begin{aligned} s_a &= (s_1 - s_2 - s_8) \\ s_b &= (s_2 - s_3 + s_7)\,. \end{aligned} \tag{2}$$

The inverter output voltage, consisting of nine discrete levels, can be expressed using the switching function in (2). It is determined by the DC source voltage and the measured capacitor voltage (v_C) as follows:

$$v_{ab} = s_a V_{in} + s_b v_C. \tag{3}$$

The grid current dynamics are equated by:

$$\frac{di_g}{dt} = -\frac{r_g}{L_g} i_g + \frac{1}{L_g}\left(V_{ab} - v_g\right), \tag{4}$$

where i_g is the measured grid current while L_g and r_g are the grid inductance and internal parasitic resistance, respectively. The measured grid voltage, v_g can be expressed as $v_g = V_{g,peak}\sin(wt)$.

Similarly, the dynamic of the capacitor voltage is given by:

$$\frac{dv_C}{dt} = -\frac{s_b}{C} i_g \tag{5}$$

The discrete form of (4) and (5) can be found by using Euler approximation assuming the signals are constant for the entire switching period T_s. The future values of the states at $(k+1)T_s$ are given by:

$$\begin{aligned} i_g(k+1) &= \left(1 - \frac{r_g}{L_g}\right) i_g(k) + \frac{T_s}{L_g}\left(v_{ab}(k) - v_g(k)\right), \\ v_C(k+1) &= v_C(k) - \frac{s_b(k) T_s}{C} i_g(k). \end{aligned} \tag{6}$$

To transfer active power from the DC source V_{in} to the grid, it is necessary to regulate the capacitor voltage to its reference value and ensure that the grid current remains close to its reference. The errors are defined as follows:

$$\begin{aligned} e_i &= i_g - i_g^* \\ e_v &= v_c - v_c^*. \end{aligned} \tag{7}$$

The future value of the gird current reference is computed by:

$$i_g^*(k+1) = \frac{3}{2} i_g(k) - \frac{1}{2} i_g(k-1) \tag{8}$$

In the following subsections, different control techniques, that are mostly applied to the CSC inverter, are discussed. All the discussed algorithms are of the finite control set type, and thus MPC, LMPC, and SMC will be used instead of FCS-MPC, FCS-LMPC, and FCS-SMC, respectively.

Algorithm 1: Claasical MPC Algorithm.

1: Measure $v_g(k)$, $i_g(k)$, $v_c(k)$
2: Calculate (6) and (8).
  for $i \leftarrow 1$ to 16 **do**
3: Calculate (9)
  end for
4: **return** minimum J_{MPC}
5: Choose the switching pair for which J_{MPC} is minimum

III. CONTROLLERS DESIGN

A. MODEL PREDICTIVE CONTROLLER (MPC)

For the CSC topology shown in Fig. 1, a finite set of control inputs ($i = 1 \ldots 16$) are listed in Table 1. It is aimed at controlling the grid current and the flying capacitor voltage, therefore, the cost function is defined as [12]

$$J_{MPC} = \lambda(v_c^* - v_c(k+1))^2 + (i_g^*(k+1) - i_g(k+1))^2. \tag{9}$$

where λ is a gain parameter allowing the summation of voltage and current values. The tuning of the gain value can be done by trial and error or using an optimization method after running different simulations with the nominal values of the system parameters ($\lambda = 0.5$ is used in the experimental results). The complete algorithm is shown in Algorithm 1.

B. LYAPUNOV-BASED MODEL PREDICTIVE CONTROLLER (LMPC)

Based on the mathematical model given in (3), (4), and (5), together with Table 1, and for the purpose of Lyapunov-based

Algorithm 2: Lyapunov-based MPC Algorithm.

Measure $v_g(k)$, $i_g(k)$, $v_c(k)$
2: Calculate Calculate (6) and (8).
for $i \leftarrow 1$ to 16 **do**
Calculate (12)
end for
4: **return** minimum J_{LMPC}
Choose (s_a, s_b) for which J_{LMPC} is minimum

model predictive control design, a positive definite cost function is selected as

$$J_{\text{LMPC}} = \frac{1}{2}K_1 e_i^2 + \frac{1}{2}K_2 e_v^2 \tag{10}$$

where K_1 and K_2 are positive constants. The basic idea here is to select the control pair (s_a, s_b), which makes the derivative of (10) negative [18]. By doing so, we are sure that the controlled system is stable according to Lyapunov's theory. Using the system equations, one may find the derivative as

$$\dot{J}_{\text{LMPC}} = e_i e_v s_b \left(\frac{K_1}{L_g} - \frac{K_2}{C}\right) + +K_2 e_v \left(\frac{1}{C} s_b \dot{i}_g^* - \dot{v}_C^*\right)$$
$$K_1 e_i \left(\frac{1}{L_g}\left[s_a V_{\text{in}} + s_b v_C - v_g\right] - \dot{i}_g^*\right) \tag{11}$$

To eliminate the common term $e_i e_v$, the gains are selected as $K_1 = \frac{K_2 L_g}{C}$, thus (11) is simplified as

$$\dot{J}_{\text{LMPC}} = \frac{K_1}{L}\Bigg(e_i\left(s_a V_{\text{in}} + s_b v_C^* - v_{ab}^*\right)$$
$$- e_v\left(\frac{1}{C} s_b i_g^*\right)\Bigg) \tag{12}$$

where v_{ab}^* is its reference value given by:

$$v_{\text{ab}}^* = v_g + r_g i_g^* + L\frac{di_g^*}{dt}. \tag{13}$$

The cost function in (12) is evaluated for all the control inputs in Table 1 and control input for the minimum cost function is selected according to the Algorithm 2.

C. SLIDING MODE CONTROLLER (SMC)

Unlike MPC and LMPC algorithms, which require the mathematical model of the controlled system, the SMC control algorithm is independent of the mathematical model of the system, and the performance depends solely on the sign of the cost function. Therefore, for designing a sliding mode (SM) controller, usually a single sliding line (σ) is defined as a linear combination of the system state errors (i.e. $\sigma(\mathbf{x}) = \boldsymbol{\alpha}^T \mathbf{x}$), but this method does not apply to the CSC topology due to complex nonlinearities that exist in this converter. Therefore, a split sliding line design is suggested in which two separate sliding functions are used to control the system dynamics [14].

The sliding lines (surfaces) are designed to operate around the origin in the steady state and they are defined as

$$\sigma_1 = e_i$$
$$\sigma_2 = e_v. \tag{14}$$

To direct the system's trajectories towards the sliding lines, a control strategy is chosen to govern the system through various control actions. Referring to (14), the following reaching condition must be valid at each time instant.

$$\sigma_1 \dot{\sigma}_1 \leq 0, \quad \text{and} \quad \sigma_2 \dot{\sigma}_2 \leq 0. \tag{15}$$

SMC is designed to operate at each sample time (T_s) with ON or OFF control input in order to satisfy the reaching condition in (15) that put in a cost function form as

$$J_1 = \sigma_1 \dot{\sigma}_1$$
$$J_2 = \sigma_2 \dot{\sigma}_2, \tag{16}$$

and evaluated for each control choice listed in Table 1. Using the system error equations in (7), and their derivatives, one can obtain the following [14], [19]

$$J_1^{(i)} = \frac{e_i}{L}\left(v_{\text{ab}} - v_{\text{ab}}^* - r_g i_g^*\right)$$
$$J_2^{(i)} = -\frac{s_b}{C} e_v i_g e_i, \tag{17}$$

where v_{ab} is the inverter terminal voltage defined in (3). Referring to the control algorithm shown in Algorithm 3, the controller first measures the grid voltage and current to calculate system error states. It then evaluates the two cost functions from equations (16) for all input pairs. At the end of each iteration, the controller checks if the capacitor voltage error is within a specified hysteresis band (h). This band allows for a small deviation in capacitor voltage, providing system flexibility without the need for gain tuning and aiming to reduce the average switching frequency [19].

If the capacitor voltage is within the hysteresis band, the controller uses only the grid current dynamic equation, selecting the input that makes J_1 negative. If the voltage is outside the band, both cost functions are considered, with the controller choosing the input pair with the least negative values for stability and reduced converter stress. If no input pair yields negative values for both cost functions, the controller selects the input where J_1 is negative and J_2 is zero. Notably, J_2 is automatically zero for $i \in 1, 4, 7$.

IV. PERFORMANCE EVALUATION

To quantitatively compare the three control strategies—MPC, LMPC, and SMC—a normalized radar chart was constructed using four key performance metrics: RMS voltage error, RMS current error, total harmonic distortion (THD), and average switching frequency. Each metric was normalized by its maximum value across all methods to ensure comparability,

$$x_{i,j}^{\text{norm}} = \frac{x_{i,j}}{\max\limits_{i}\left(x_{i,j}\right)}, \tag{18}$$

Algorithm 3: SMC Algorithm.

Measure $v_g(k)$, $i_g(k)$, $v_c(k)$
Calculate e_i, e_v, v^*_{ab}
for $i \leftarrow 1$ to 16
  Calculate (17)
end for
if $e_v > h$ **then**
  Choose (s_a, s_b) for which $J_1(i) < 0$
else if $J_1(i) < 0$ & $J_2(i) < 0$ **then**
  Select the corresponding (s_a, s_b) pair
else
  Choose (s_a, s_b) for which $J_1(i) < 0$ & $J_2(i) = 0$
end if

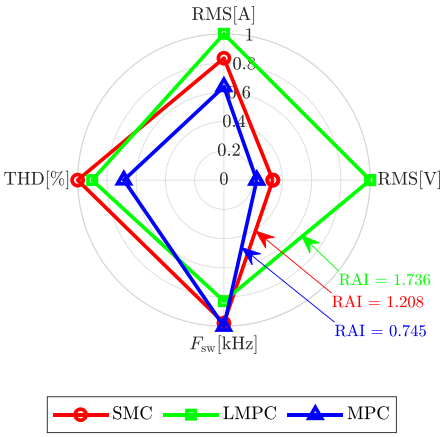

FIGURE 2. Normalized radar chart of SMC, LMPC, and MPC across multiple control metrics under steady state conditions.

where:

- $x_{i,j}$ is the value of metric j for method i,
- $x^{\text{norm}}_{i,j}$ is the normalized value.

and the area enclosed by the radar polygon was computed for each method i

$$\text{RAI}_i = \frac{1}{2}\left|\sum_{k=1}^{N}\left(x_k y_{k+1} - y_k x_{k+1}\right)\right|, \tag{19}$$

with:

$$x_k = x^{\text{norm}}_{i,k}\cos(\theta_k),$$
$$y_k = x^{\text{norm}}_{i,k}\sin(\theta_k),$$
$$\theta_k = \frac{2\pi(k-1)}{N}, \quad (x_{N+1}, y_{N+1}) = (x_1, y_1).$$

The polygon area, referred to as the Radar Area Index (RAI), serves as a performance indicator: the smaller the area, the better the overall performance across all metrics.

Refer to Fig. 2, the computed RAIs values are showing clearly that MPC provides the most balanced and superior performance. SMC exhibits moderate results, while LMPC suffers from higher voltage deviation and switching frequency, resulting in the largest performance area. This area-based analysis provides a simple yet effective tool to evaluate multi-objective performance, especially when no single metric dominates the others and scalarization via weighted cost functions is to be avoided. Keep in mind that SMC and LMPC-based methods require no gain tuning compared to MPC.

Fig. 3 shows a +30% and −30% mismatch in the actual inductor value compared to its value used in the simulation. A numerical value for RAI is calculated for each method where MPC has kept the best RAI index value across all other methods. In case of a +30% mismatch in L_g, one may notice that LMPC has the lowest average switching frequency on the cost of higher RMS error in the capacitor voltage error, whereas, MPC and SMC have similar switching frequency and RMS current error. LMPC has the highest THD value, followed by SMC and MPC. A better performance of the LMPC compared to other methods can be seen when we have a −30% mismatch in the inductor value, LMPC can still have the lowest average switching frequency, a smaller THD (and thus a smaller current RMS error), at high RMS voltage error.

Another test is made to compare all the methods together, a capacitor mismatch with a +40% and −40% is simulated for all the control algorithms. The overall performance of RAI is given in Fig. 4 (results are obtained under nominal operating conditions for $h = 1V$ for SMc, and $\lambda = 0.5$ for MPC algorithm). One can see that MPC has the smallest RAI index, thus the best performance index, but it is also important to point out that it has the highest switching frequency. One important observation is that, when comparing LMPC and MPC in case of +40% mismatch in C, one can observe that both methods have similar performance except for the fact that MPC can still keep the capacitor voltage controlled better (closer to its reference value).

To ensure a fair comparison among the different control strategies, all controllers were carefully tuned to achieve their best performance with respect to key metrics: grid current THD, capacitor-voltage RMS error, and average switching frequency. Additional simulations were conducted under equalized performance constraints. The results are summarized in the normalized radar charts shown in Fig. 5: Fig. 5(a) shows the controllers tuned to achieve equal THD, where MPC yields the smallest radar area index (RAI) followed by SMC and LMPC; Fig. 5(b) shows the controllers tuned to achieve equal capacitor-voltage RMS error, highlighting that MPC still provides the lowest RAI while SMC achieves the smallest current RMS error; and Fig. 5(c) shows the controllers tuned for equal average switching frequency, illustrating that MPC achieves the best current quality, LMPC maintains inherent stability without gain tuning, and SMC offers robustness. These results demonstrate that performance comparisons are sensitive to parameter selection, and each controller exhibits distinct advantages under different performance constraints.

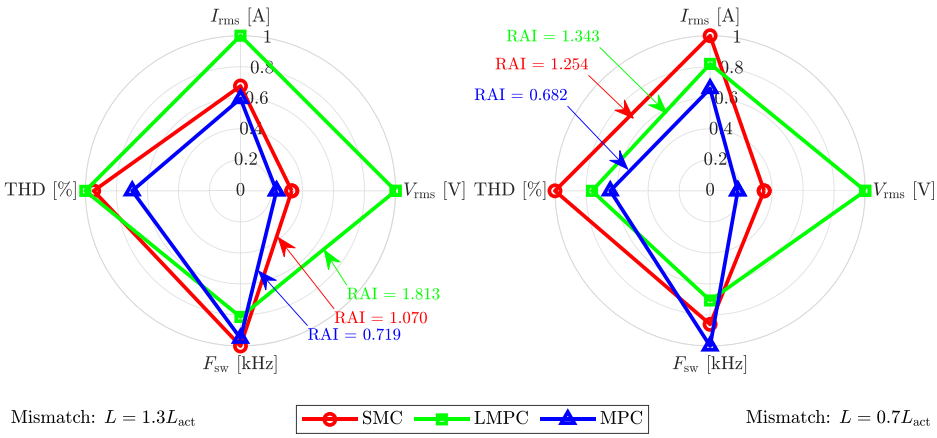

FIGURE 3. Normalized radar chart of SMC, LMPC, and MPC across multiple control metrics in case of inductance mismatch.

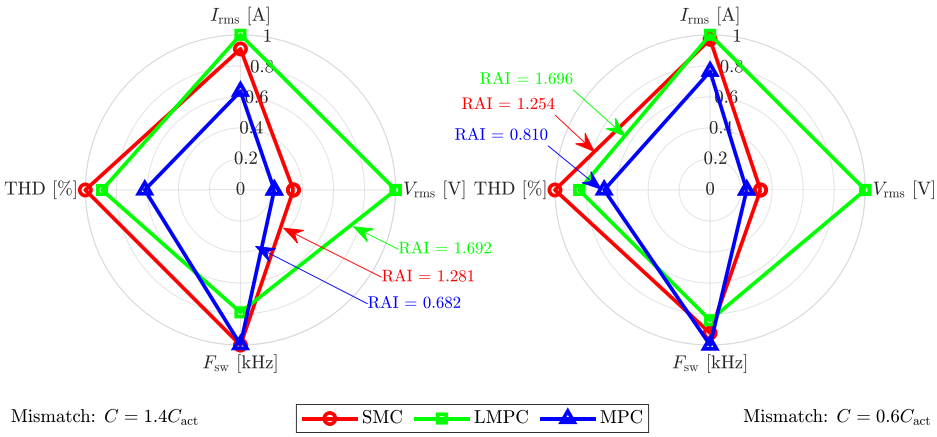

FIGURE 4. Normalized radar chart of SMC, LMPC, and MPC across multiple control metrics in case of capacitance mismatch.

For all three control strategies, parameters are selected based on clear and consistent design principles rather than numerical optimization for a specific operating point. This ensures a transparent and fair comparison, allowing general performance trends and practical trade-offs among MPC, LMPC, and SMC to be systematically evaluated under identical conditions.

V. REAL-TIME SIMULATION AND RESULTS

To evaluate and compare the performance of MPC, LMPC, and SMC, MATLAB toolbox and a real-time simulation model of the CSC inverter were used. real-time simulation model was developed and implemented on the Opal-RT OP4610XG simulator. The system was tested under various operating conditions, and the corresponding results were recorded. Table 2 summarizes the parameters used in the real-time implementation tests.

A simulation test using MATLAB toolbox was conducted in which the capacitance value was increased by 30% while the inductance value was decreased by 30%. As shown in the steady-state waveforms in Fig. 6, both the SMC and MPC successfully generate all nine output voltage levels, whereas

TABLE 2 System Parameters for Grid-Connected Mode Operation

Parameter	Value
Input voltage, v_{in}	360 V
Line frequency, f_{line}	50 Hz
Grid voltage $v_{g,\text{rms}}$	240 V
Line Filter , L_g, r_g	5 mH, 0.01 Ω
Flying capacitors, C	1 mF
Sampling period, T_s	20 μs
Allowable voltage error h	1 V
Control parameter λ	0.5

the LMPC fails to maintain all levels at certain instants. This behavior is expected, since the LMPC does not include tunable gains and its control action strictly follows the predefined Lyapunov-based cost function. In addition, another test was performed in which a severe voltage dip was applied to the grid. Specifically, the grid voltage is reduced by 50% at $t = 0.445$ s and then restored to its nominal value at $t = 0.5$ s. The results of this test are presented in Fig. 7. This scenario further demonstrates that all three controllers are able to maintain stable operation and recover quickly from a severe

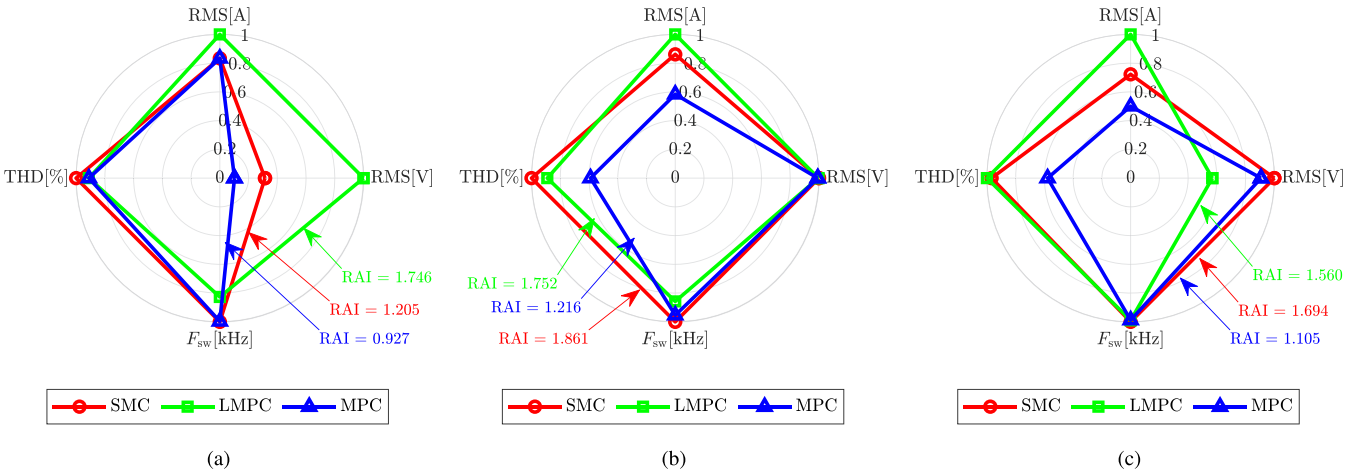

FIGURE 5. Comparison of normalized radar values for the proposed algorithms under different constraints: (a) equal THD value, (b) equal capacitor RMS error, and (c) equal average switching frequency.

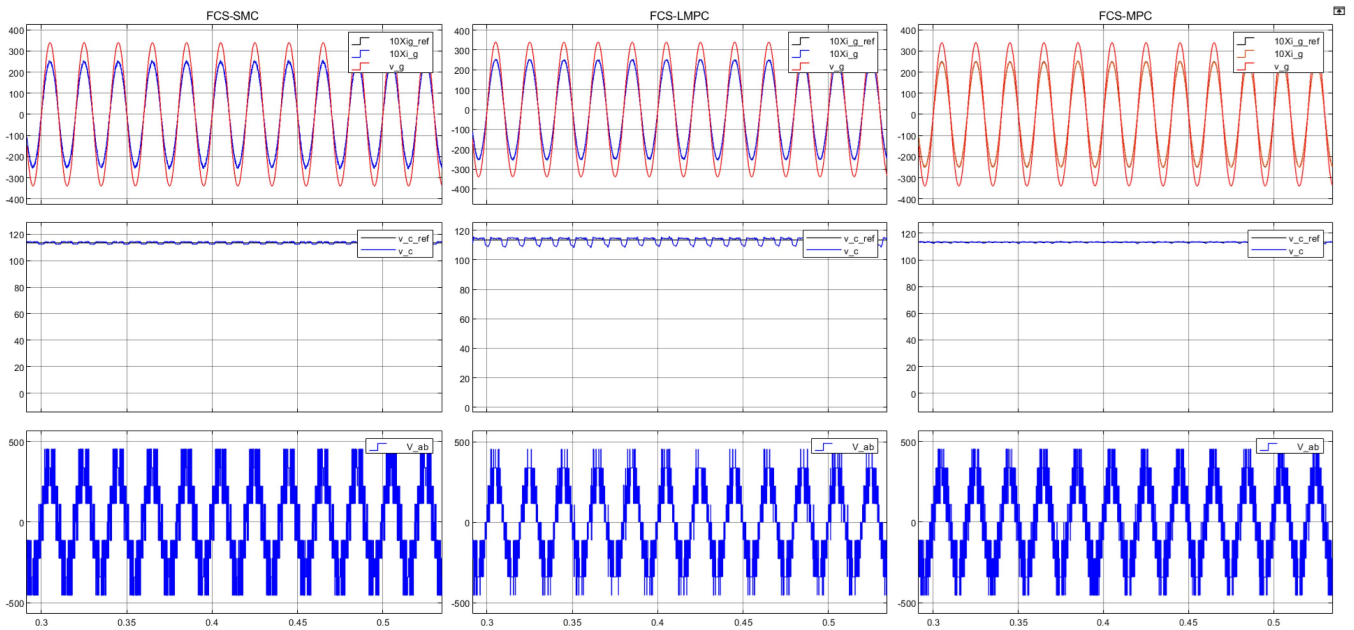

FIGURE 6. Steady-state simulation results for the different control algorithms for $L_{act} = 0.7 \times L$ and $C_{act} = 1.3 \times C$.

disturbance, enabling a clear comparison of their disturbance rejection capabilities.

Opal-RT simulator is also used in real-time simulation. In the first test, steady-state results were recorded and are presented in Fig. 8. The results indicate that MPC and LMPC exhibit superior current control with lower harmonic distortion. However, SMC outperforms the other controllers in maintaining capacitor voltage balance and effectively generating nine voltage levels at the output. This can be explained by referring to Algorithm 3, which operates as a current controller unless the capacitor voltage error exceeds the allowed hysteresis width (here $h = 1V$). Having the voltage error hysteresis adds an extra degree of freedom in the control design problem which distinguishes SMC from the other two algorithms. In contrast, MPC and LMPC utilize a cost function that combines voltage and current errors, aiming to minimize both simultaneously. Notably, in MPC, the errors are coupled through weighting factors, whereas in LMPC, the weights are inherently canceled out in the cost function design. Additionally, the SMC algorithm is expected to result in a higher switching frequency, while MPC and LMPC do not require frequent switching, leading to a lower average switching frequency. This explanation is valid for the following results too.

One may observe that SMC has the smallest voltage ripple (limited to 1 V, which can be adjusted to a different value based on the designer's preference), followed by LMPC and MPC, respectively. When comparing MPC and LMPC, it is

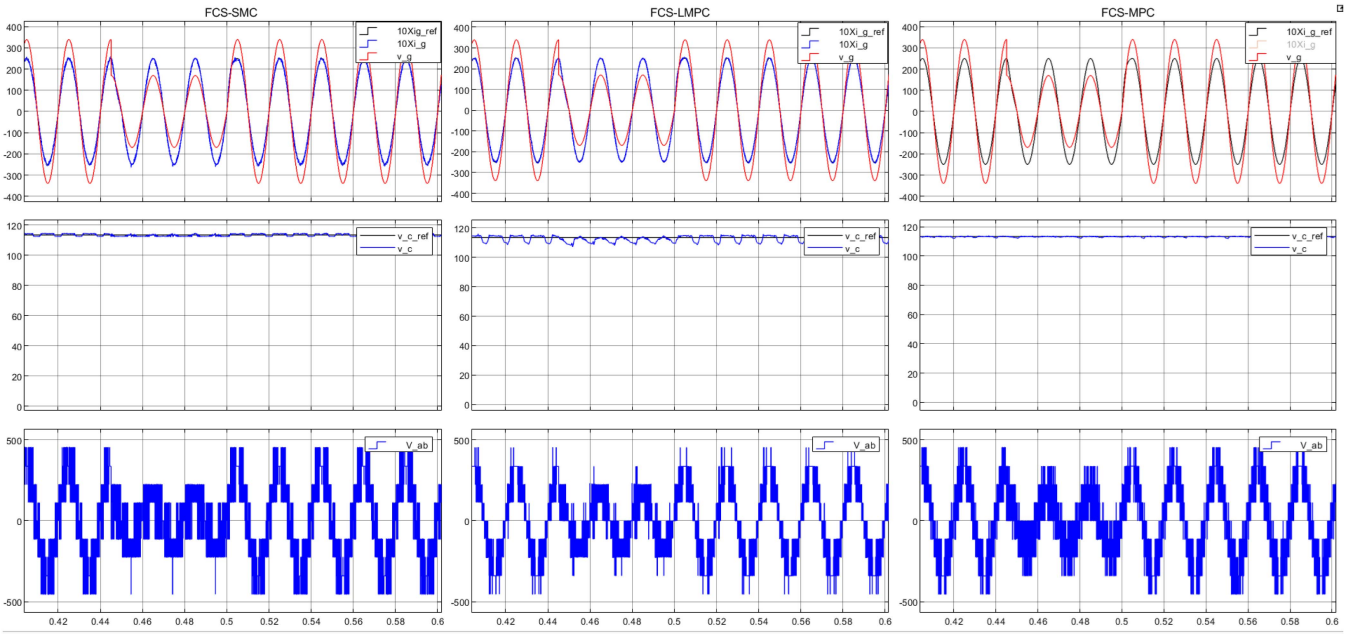

FIGURE 7. Simulation results under steady state for SMC, LMPC and MPC during 50% voltage drop in the grid voltage.

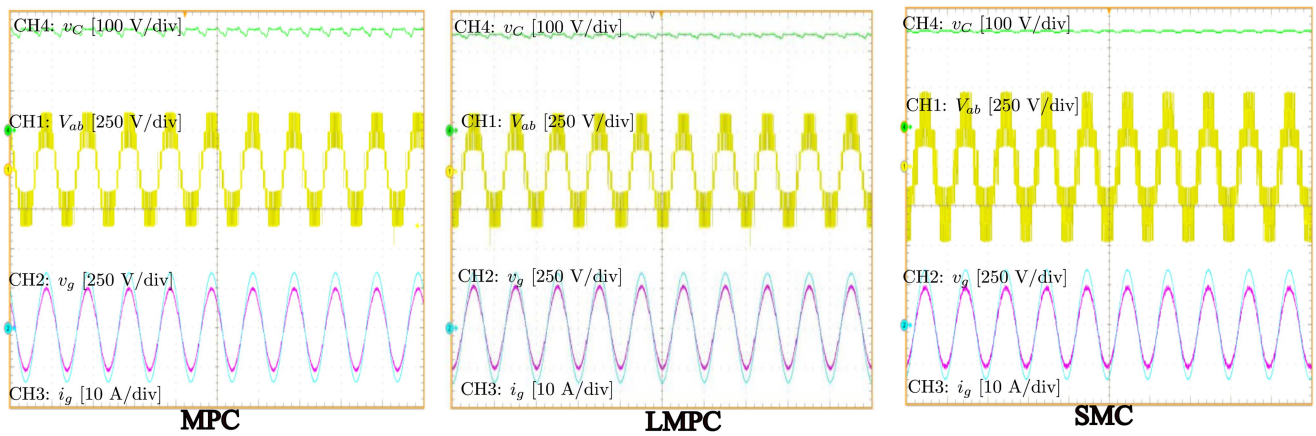

FIGURE 8. Steady-state experimental results for different control algorithms during active power injection to the grid.

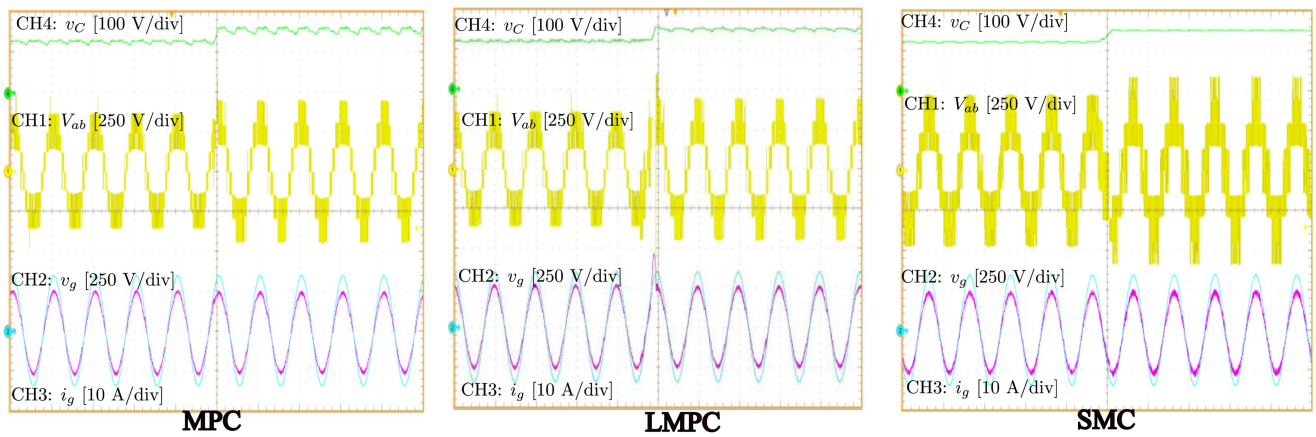

FIGURE 9. Dynamic response to a change in DC source voltage from 360 V to 450 V.

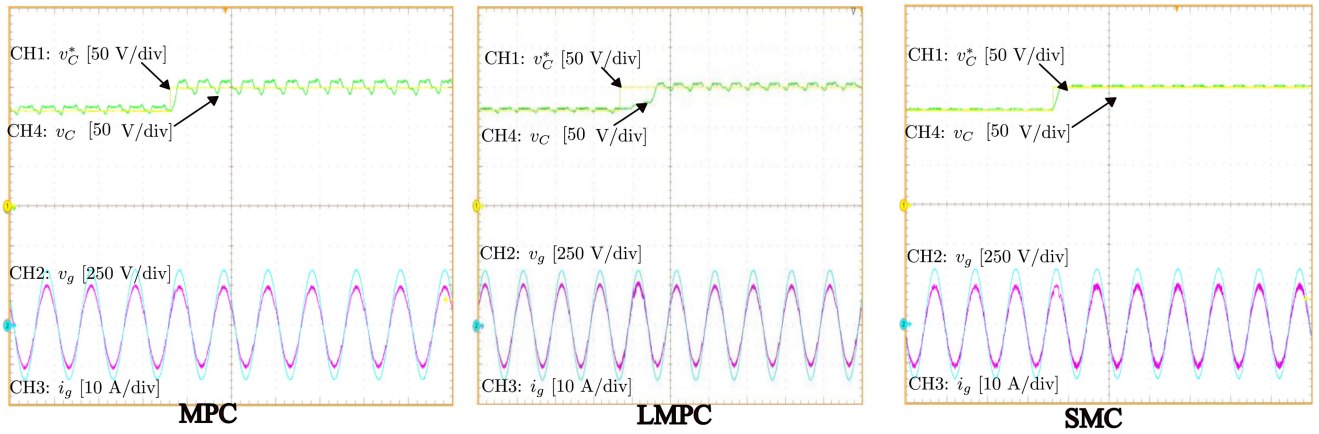

FIGURE 10. Dynamic response to a change in DC source voltage from 360 V to 450 V.

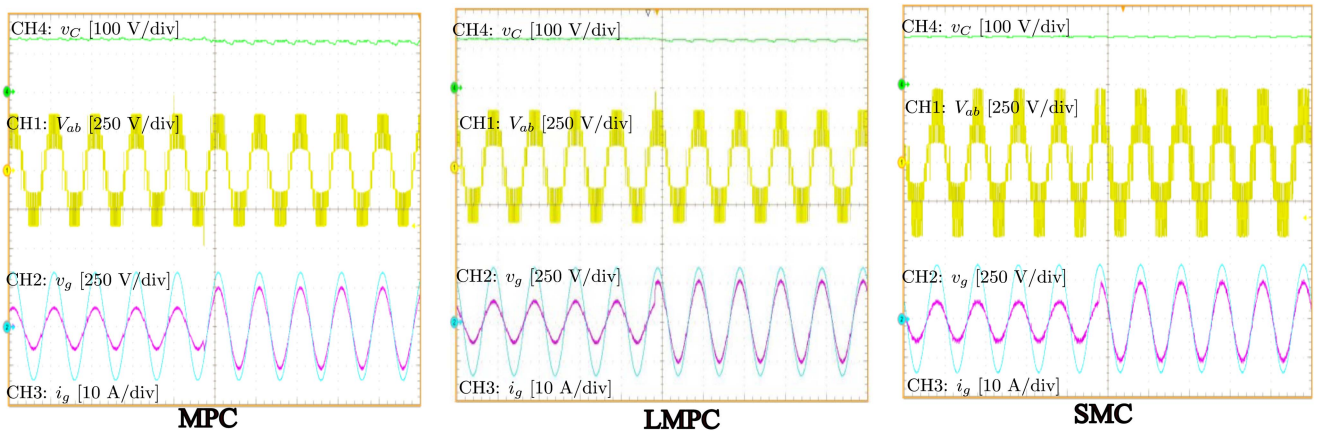

FIGURE 11. Grid current dynamic response (i_g^* changes from 5 A to 10 A).

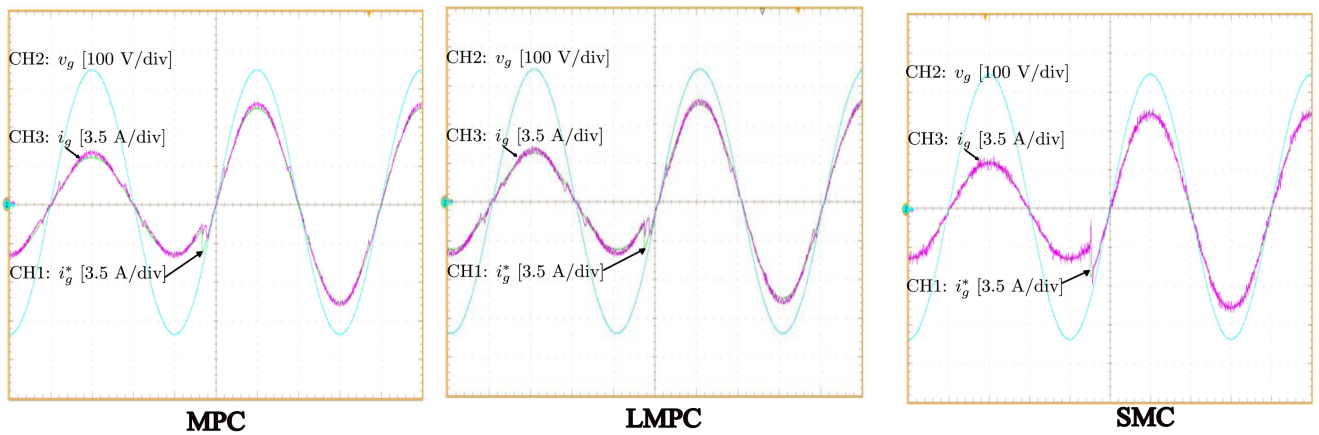

FIGURE 12. Grid current dynamic response (i_g^* changes from 5 A to 10 A).

clear that their performance is similar, with the exception that LMPC demonstrates a lower voltage ripple. However, this does not necessarily imply superior performance unless both algorithms are evaluated under the same average switching frequency—a comparison that was not conducted in this study and is deemed unnecessary, as similar performance has been previously demonstrated [20], [20]. This observation holds true for the subsequent results as well.

In the second test, the DC source voltage was increased from 360 V to 450 V, resulting in a corresponding adjustment

of the capacitor voltage from 120 V to 150 V (maintaining one-third of the DC source voltage). The results, shown in Figs. 9 and 10, reveal that LMPC responds slower than both MPC and SMC as depicted in Fig. 9. Furthermore, an analysis of the inverter voltage waveform, shown in Fig. 10, reveals that both LMPC and MPC generate seven voltage levels even at higher operating voltages, whereas SMC consistently produces nine voltage levels across all operating conditions. This difference arises because SMC primarily functions as a current controller (as long as the voltage is controlled within a 1 V error band), unlike MPC and LMPC. Additionally, it is evident that SMC requires a higher switching frequency, as switching is triggered whenever the current error changes sign.

In the final test, a step change in current amplitude was introduced to evaluate the dynamic performance of the controllers in tracking the reference current value. Specifically, the current reference was increased from 5 A to 10 A, and the corresponding results are presented in Figs. 11 and 12. The results indicate that the system remains stable despite the abrupt current variation. Additionally, all controllers effectively track the new reference value without compromising performance.

VI. CONCLUSION

This paper presents a comparative analysis of three advanced control strategies — Model Predictive Control (MPC), Lyapunov-based MPC (LMPC), and Sliding Mode Control (SMC) — applied to a grid-connected 9-level Crossover Switch Cell (CSC) converter. Using real-time implementation on the Opal-RT platform, the controllers were evaluated under various operating conditions, including steady-state performance, transient response to DC voltage variations, and changes in current reference. The presented results demonstrated that MPC exhibits fast response times, precise current control, and significantly reduced total harmonic distortion (THD), all while maintaining a reasonable switching frequency and offering tunable performance across different power levels. LMPC achieves similar performance without the need for tuning, but at the cost of slower dynamics, although it ensures system stability. SMC, on the other hand, provides a fast dynamic response, strong robustness against parameter variations and disturbances, and effective capacitor voltage balancing. However, it operates at a higher switching frequency. Unlike MPC and LMPC, SMC functions independently of the system's mathematical model and introduces an additional degree of freedom for controlling specific variables, making it a flexible alternative for applications that require enhanced adaptability. These findings provide practical guidelines for selecting the most suitable control approach based on specific application requirements: MPC is ideal for applications requiring minimal THD and high power quality; SMC offers better resilience to disturbances; and LMPC is a viable alternative for stability-focused designs. Future work could explore hybrid control strategies to enhance efficiency, mitigate chattering in SMC, and further optimize computational resources in MPC-based methods.

REFERENCES

[1] P. Roy, J. He, T. Zhao, and Y. V. Singh, "Recent advances of wind-solar hybrid renewable energy systems for power generation: A review," *IEEE Open J. Ind. Electron. Soc.*, vol. 3, pp. 81–104, 2022.

[2] F. Z. Peng, C.-C. Liu, Y. Li, A. K. Jain, and D. Vinnikov, "Envisioning the future renewable and resilient energy grids—A power grid revolution enabled by renewables, energy storage, and energy electronics," *IEEE J. Emerg. Sel. Topics Ind. Electron.*, vol. 5, no. 1, pp. 8–26, Jan. 2024.

[3] H. Abu-Rub, M. Malinowski, and K. Al-Haddad, "Multilevel converter/inverter topologies and applications," in *Power Electron. Renewable Energy Syst., Transp. Ind. Application*. Piscataway, NJ, USA: IEEE Press, 2014, pp. 422–462.

[4] J. Rodriguez, J.-S. Lai, and F. Z. Peng, "Multilevel Inverters: A survey of topologies, controls, and applications," *IEEE Trans. Ind. Electron.*, vol. 49, no. 4, pp. 724–738, Aug. 2002.

[5] M. Trabelsi, H. Vahedi, and H. Abu-Rub, "Review on single-DC-source multilevel inverters: Topologies, challenges, industrial applications, and recommendations," *IEEE Open J. Ind. Electron. Soc.*, vol. 2, pp. 112–127, 2021.

[6] A. Nabae, I. Takahashi, and H. Akagi, "A new neutral-point-clamped PWM inverter," *IEEE Trans. Ind. Appl.*, vol. IA- 17, no. 5, pp. 518–523, Sep. 1981.

[7] C. Wang, J. Xu, X. Pan, W. Gong, Z. Zhu, and S. Xu, "Impedance modeling and analysis of series-connected modular multilevel converter (MMC) and its comparative study with conventional MMC for HVDC applications," *IEEE Trans. Power Del.*, vol. 37, no. 4, pp. 3270–3281, Aug. 2022.

[8] S. K. Patro and A. Shukla, "Modular directed series multilevel converter for HVDC applications," *IEEE Trans. Ind. Appl.*, vol. 56, no. 2, pp. 1618–1630, Mar./Apr. 2020.

[9] T. Meynard and H. Foch, "Multi-level choppers for high voltage applications," *EPE J.*, vol. 2, no. 1, pp. 45–50, 1992.

[10] M. Trabelsi and L. Ben-Brahim, "Experimental photovoltaic power supply based on flying capacitors multilevel inverter," in *Proc. Int. Conf. Clean Elect. Power*, 2011, pp. 578–583.

[11] Y. Ounejjar, K. Al-Haddad, and L.-A. Gregoire, "Packed U cells multilevel converter topology: Theoretical study and experimental validation," *IEEE Trans. Ind. Electron.*, vol. 58, no. 4, pp. 1294–1306, Apr. 2011.

[12] M. Trabelsi, S. Bayhan, K. A. Ghazi, H. Abu-Rub, and L. Ben-Brahim, "Finite-control-set model predictive control for grid-connected packed-U-cells multilevel inverter," *IEEE Trans. Ind. Electron.*, vol. 63, no. 11, pp. 7286–7295, Nov. 2016.

[13] H. Vahedi, K. Al-Haddad, Y. Ounejjar, and K. Addoweesh, "Crossover switches cell (CSC): A new multilevel inverter topology with maximum voltage levels and minimum DC sources," in *Proc. 39th Annu. Conf. IEEE Ind. Electron. Soc.*, 2013, pp. 54–59.

[14] H. Makhamreh, M. Trabelsi, and A. N. Alquennah, "Model-independent sliding mode control for grid-connected crossover switches cell inverter with reduced switching frequency," in *Proc. 49th Annu. Conf. IEEE Ind. Electron. Soc.*, 2023, pp. 1–6.

[15] X. Yang, Z. Li, T. Q. Zheng, X. You, and P. Kobrle, "Virtual impedance sliding mode control-based MMC circulating current suppressing strategy," *IEEE Access*, vol. 7, pp. 26229–26240, 2019.

[16] A. N. Alquennah, M. Trabelsi, K. Rayane, H. Vahedi, and H. Abu-Rub, "Real-time implementation of an optimized model predictive control for a 9-level CSC inverter in grid-connected mode," *Sustainability*, vol. 13, no. 15, 2021, Art. no. 8119. [Online]. Available: https://www.mdpi.com/2071-1050/13/15/8119

[17] A. Alquennah, M. Trabelsi, and H. Vahedi, "FCS-MPC of grid-connected 9-level crossover switches cell inverter," in *Proc. 46th Annu. Conf. IEEE Ind. Electron. Soc.*, 2020, pp. 2430–2435.

[18] M. Trabelsi, H. Makhamreh, A. N. Alquennah, and H. Vahedi, "Lyapunov-based model predictive control for stable operation of a 9-level crossover switches cell inverter in grid connection mode," in *Proc. 49th Annu. Conf. IEEE Ind. Electron. Soc.*, 2023, pp. 1–6.

[19] H. Makhamreh, M. Trabelsi, O. Kükrer, and H. Abu-Rub, "An effective sliding mode control design for a grid-connected PUC7 multilevel inverter," *IEEE Trans. Ind. Electron.*, vol. 67, no. 5, pp. 3717–3725, May 2020.

[20] H. Makhamreh, M. Sleiman, O. Kükrer, and K. Al-Haddad, "Lyapunov-based model predictive control of a PUC7 grid-connected multilevel inverter," *IEEE Trans. Ind. Electron.*, vol. 66, no. 9, pp. 7012–7021, Sep. 2019.

HAMZA MAKHAMREH (Senior Member, IEEE) received the B.Sc. degree in electrical engineering from Palestine Technical University (PTU–Kadoorie), Tulkarem, Palestine, in 2009, and the M.Sc. and Ph.D. degrees in electrical and electronic engineering from Eastern Mediterranean University (EMU), Gazimağusa, Cyprus, in 2019. From 2019 to 2021, he was with the Department of Electrical and Electronics Engineering, Middle East Technical University (METU-NCC), Ankara, Türkiye, and the Department of Mechanical Engineering with EMU. Since 2021, he has been with the Department of Electrical and Electronics Engineering, Özyeğin University, Istanbul, Turkey. His research interests include power electronics, energy conversion, and control of power electronic systems. Dr. Makhamreh was the recipient of the Best Paper Award at the 2023 IEEE International Conference on Predictive Control of Electrical Drives and Power Electronics (PRECEDE), Wuhan, China.

MOHAMED TRABLESI (Senior Member, IEEE) received the B.Sc. degree in industrial informatics and automation from INSAT, Tunis, Tunisia, in 2006, and the M.Sc. degree in automated systems and the Ph.D. degree in energy systems from INSA Lyon, France, in 2006 and 2009, respectively. From 2009 to 2018, he held several research and academic positions with Qatar University, Doha, Qatar, and Texas A&M University at Qatar, Ar-Rayyan, Qatar, where he contributed to large-scale research projects on Renewable Energy Integration, Advanced Power Converters, and Smart Grids. In 2018, he joined the Kuwait College of Science and Technology (KCST), Kuwait City, Kuwait, where he is currently a Full Professor and the Head of the Electronics and Communications Engineering Department. Prof. Trabelsi has an internationally recognized research profile in Power Electronics, Smart Grids, Renewable and Energy Harvesting Systems, Electric Vehicles, and AI-based Control and Energy Management. He was the Principal Investigator on several internationally funded projects, supported by QNRF, FCDO, KFAS and other agencies, with a cumulative budget of seven million USD. He is ranked among the Top 2% of highly cited researchers worldwide (Stanford University ranking) for four consecutive years from 2021 to 2025 in the fields of Electrical and Electronic Engineering and Energy. He is also an Associate Editor for IEEE TRANSACTIONS ON INDUSTRIAL ELECTRONICS, Secretary of the IEEE IES Technical Committee on Power Electronics, and Member of the IEEE IES Chapter and Joint Chapter Program Committee. He is also actively involved in organizing International IEEE and SPRINGER Conferences and organizing Special Sessions in top IEEE conferences.

HANI VAHEDI (Senior Member, IEEE) received the Ph.D. (Hons.) degree from École de Technologie Supérieure (ÉTS), Université du Québec, Montréal, QC, Canada, in 2016. After seven years in the industry working as a Power Electronics Designer and later as a Chief Scientific Officer, he joined the Delft University of Technology, Delft, the Netherlands, as an Assistant Professor to advance electrification for the clean energy transition. He leads TU Delft's 24/7 Energy Hub with The Green Village, an operational microgrid that integrates renewables, green hydrogen production, and hybrid energy storage systems. He has authored more than 100 IEEE conference and journal papers, a Springer Nature book, and a book chapter published by Elsevier. His research interests include multilevel power converter topologies, modulation and control, and applications in smart grids, renewable energy conversion, EV charging, green hydrogen production through electrolysis, and fuel-cell systems. He has been an active Member of the IEEE Industrial Electronics Society (IES) since 2012, is on the local organizing committee for IECON12 in Montreal, acting as Students and Young Professionals Chair for numerous IES-sponsored conferences from 2016 to 2024, and is also a Technical Program Chair (GreenTech Cluster) for IECON25 in Madrid, and Special Sessions Chair for IECON26 in Doha. He currently manages the IES Chapters & Joint Chapters Program. He is an Associate Editor for IEEE TRANSACTIONS ON INDUSTRIAL ELECTRONICS, IEEE OPEN JOURNAL OF THE INDUSTRIAL ELECTRONICS SOCIETY, and IEEE OPEN JOURNAL OF POWER ELECTRONICS. Dr. Vahedi is the Inventor of the five-level Packed U-Cell (PUC5) converter, holds several U.S. and international patents, and transferred this technology to industry, assisting in the development of a bidirectional EV charger based on his invention. He was awarded ÉTS's Best Ph.D. Thesis Award from 2016 to 2017.